Structure changes in two chosen metallic materials exposed to molten LiF-NaF eutectic mixture – model of corrosion behaviour

L. Král[1], J. Čermák[1*], O. Matal[2], T. Šimo[2], L. Nesvadba[2], M. Jílek[3]

[1]*Institute of Physics of Materials AS CR, v. v. i., Žižkova 22, CZ-616 62 Brno, Czech Republic*
[2]*Energovýzkum, spol. s r.o., Božetěchova 17, CZ-612 00 Brno, Czech Republic*
[3]*Inženýrská kancelář Jílek, Manětínská 8, CZ-323 00 Plzeň, Czech Republic*

Abstract

This work is devoted to the study of changes of structure and chemical composition of two candidate materials for high-temperature power engineering. Materials are studied before and after their exposure to molten mixture 60 mol.% LiF + 40 mol.% NaF at temperature 953 K for exposure times 100, 300 and 1000 h. The exposition was carried out in a quasidynamic regime that simulated the flux of the coolant (the mixture of salts) in the pipeline. In Ni-alloy Ni-6W-9Mo-1.7Ti-7Cr (wt.%) severe corrosion damage was observed in the surface layer of thickness of about 100 μm. In Ni-coated ferrite steel CSN 411523, elements redistribution close to the interface between the Ni layer/steel substrate was described by a simple model. The Ni layer showed excellent resistance against the corrosion, but its perforation and subsequent local damage of the substrate were also observed.

K e y   w o r d s: steels, nickel alloys, corrosion, diffusion, coating

1. Introduction

Fluoride salts are promising coolant in the Very High Temperature Reactors (VHTR) of the Generation IV that operate typically as combined cycle plants for electricity/heat production [1]. Often they are designed, more specifically, for electricity/hydrogen production generated by thermo-chemical water splitting method (IS process) [2].

Up to date, the most frequently used coolant in VHTR is He that offers several advantages. Before all, it does not transform to radioactive nuclides in the core and, as an inert gas, it does not degrade chemically the material of components at pressures up to 10 MPa. A mixture of molten fluoride salts on the other hand (e.g., LiF + NaF), transforms to relative short-living radioactive nuclides only and, moreover, it avoids the high-pressure gas media in the cooling system. When an accident occurs, molten salts (LS) also offer better retention of fission products. In this way, the use of molten salts as a coolant in nuclear applications supports the concept of passive safety of the system with negligible increased risk due to their neutron activation.

The cooling of LS-VHTR (at pressures up to 0.1–0.2 MPa) with molten salts, however, brings new problems connected with high-temperature corrosion that is not fully understood up to now and hence that should require more research. It is interesting to note that the molten fluoride salts may be also useful as a liquid first wall in fusion-energy reactor [3] where the corrosion processes are of primary importance as well.

Behaviour of construction materials for heat transmission in VHTR, characteristics of coolants and interaction between the coolant and the pipeline material is in the focus of interest of both researchers and engineers in last years: Microstructure and mechanical properties of special Ni-based alloys for power generation were previously studied, e.g., in [4–7] and protective coatings for high-temperature nuclear applications were studied in [8]. The characteristics (density, surface tension, viscosity and melting temperatures) of various cooling salt mixtures see for example in [9]. Interaction between coolant (mostly: molten fluorides, chlorides, sulphides and carbonates) and Fe-based ma-

---

*Corresponding author: tel.: +420 532 290 422; fax: +420 541 218 657; e-mail address: cermak@ipm.cz

terials can be found in papers [10–12], interaction of salts with Fe-based materials (stainless steels) is studied for example in [13–18].

Corrosion of Ni, Fe, Co, and their alloys in fluoride melts was reviewed, e.g., in [19, 20], corrosion resistance of Ni-based alloys in fluoride melts was investigated in [21] and corrosion and other characteristics of candidate molten salt coolants for heat-transfer loops were assessed in reports [22, 23].

It is commonly accepted that corrosion mechanism of metals in molten salts is similar to that in electrolytes [24]. Contrary to the fact that partial radial distribution curves of cation-anion pairs show distinct maximums [25], the salt melts can be understood as a mixture of ions. Separated motion of cations and anions that manifests itself in relative good electrical conductivity of salt melts can be taken as an indirect evidence of dissociation of the salt molecules (see, e.g., dynamic dissociation model proposed in [26]). Hence, the mechanism of metals corrosion in salt melts consists in general of two steps [24]: the first one is an anodic reaction that is an oxidation of metal M at the solid surface (removal of z electrons e from the metal atom M) by aniont A^- from the melt

$$M + z\,A^- \rightarrow M^{z+} \cdot z\,A^- + z\,e. \tag{1}$$
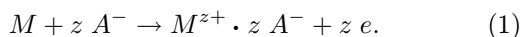
Solvated cationt of metal ($M^{z+} \cdot z\,A^-$) is transferred into the melt and free electrons are bound in the subsequent cathode reaction to a depolarisator D,

$$D + z\,e \rightarrow \left(D^{z+} \cdot z\,e\right). \tag{2}$$
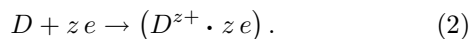
General scheme of oxidation mechanism described by Eqs. (1), (2) may be complicated considerably when impurities enter the play. Oxygen, for example, takes part in oxide reactions that should be considered simultaneously [24].

Although much effort has been devoted to the study of corrosion of pipeline material in molten fluoride salts [22, 23], there are still a lot of open questions left for further research. The present work continues our previous study [27] devoted mainly to the analysis of LiF + NaF + RbF salt bath after the contact with material of the pipeline at high temperature. Present paper deals with the composition and structure changes of the components material itself after its exposition to molten mixture LiF + NaF (60 : 40 by mol.%) at temperature 953 K and for exposure times up to 1000 h.

2. Experimental procedure

2.1. Experimental materials
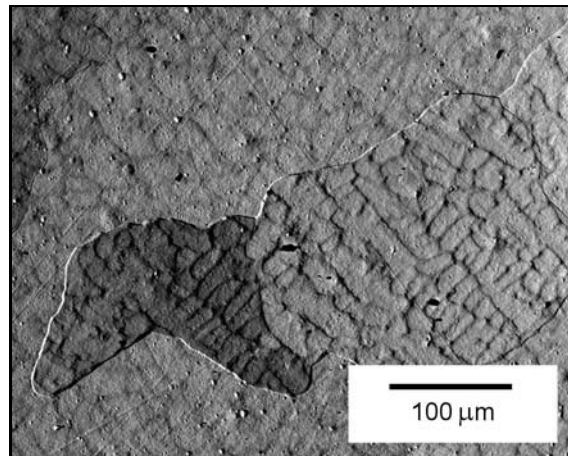
Two candidate materials were tested: i) Ni-based

Fig. 1. SEM micrograph showing the treated alloy N. Residuals of the cast structure in the grains can be seen (light – dendrites, dark – interdendritic matrix). Etched in HCl (100) – H$_2$SO$_4$ (5) – CuSO$_4$ (20), room temperature, 10 s.

alloy Ni-6W-9Mo-1.7Ti-7Cr (in wt.%) and ii) ferrite steel (CSN 411523) covered by Ni protective layer of thickness of about 100 µm. The former material will be referred to as N, the latter one as F henceforth in the text.

Alloy N was prepared from pure components (technical purity – 3N warranted) by induction melting in Ar protective atmosphere and casting into a hot copper mould. The weight of the charge was 350 g. The ingot was machined down to a cylinder ⌀ 20 × 90 mm and annealed in Ar at 1273 K for 24 h. The structure after the treatment consisted of irregular grains with grain size of the order of 10^2–10^3 µm – see Fig. 1. It was proven that the grain boundaries were well stable during the corrosion tests. Interior of the grains was formed by residuals of dendrites. It is obvious in Fig. 1 that typical distance between the dendrite axes was 40 µm. It was found by X-ray microanalysis that the dendrites were slightly enriched on tungsten ($c_{\text{dendr}}^{\text{W}}/c_{\text{interdendr}}^{\text{W}} \sim 1.5$; in wt.%) and depleted on Ti and Mo ($c_{\text{dendr}}^{\text{Ti}}/c_{\text{interdendr}}^{\text{Ti}} \sim 0.8$; $c_{\text{dendr}}^{\text{Mo}}/c_{\text{interdendr}}^{\text{Mo}} \sim 0.9$; in wt.%). Cr and Ni were distributed almost uniformly both in dendrites and in inter-dendrite matrix. Such a character of segregation was not changed during corrosion tests.

Base material of alloy F is equivalent to Euro-norm EN 10025-90 or EN 1002593. It was used in as-received state as a substrate for Ni deposition. The mean grain size of F was 20–50 µm. The Ni layer with thickness 100–200 µm was deposited electrochemically. The needle-like structure of Ni layer in F can be seen in Fig. 2.

2.2. Salt bath

Eutectic composition LiF + NaF (60 : 40 by mol.%

Ta b l e 1. Concentrations of impurities in LiF + NaF salt mixture obtained by ICP (in wt.ppm)

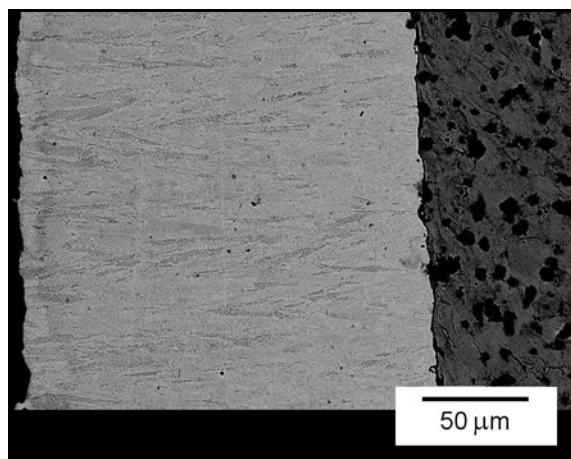| P	S	Mn	Si	Fe	Cr	Ni	Mo	Ti	Al	Cu	Co	W	V
< 10	10	< 10	720	40	< 10	10	< 10	< 10	200	< 10	< 10	< 10	< 10

Fig. 2. SEM micrograph of sample F before the exposition in molten salts. Right – steel substrate; left – Ni layer; left margin – free surface. Etchant – the same as in Fig. 1.
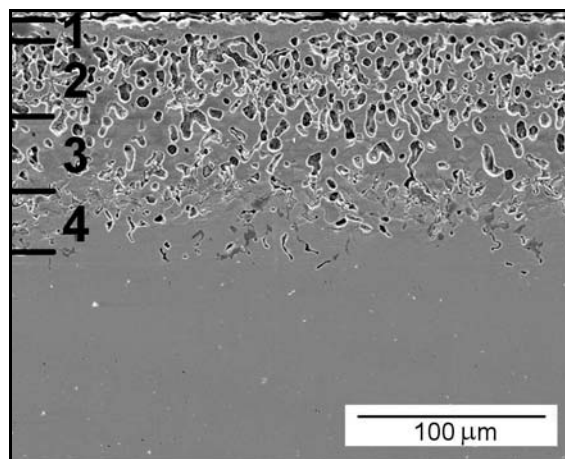

Fig. 3. SEM micrograph of alloy N after the corrosion test 953 K/1000 h showing the damaged surface layer. For numbers – see text.

[23]) was purchased by Sigma Aldrich. Chemical composition of the base elements according to the certificate of delivery was Li – 12.9, Na – 28.4 and F – 58.7. Concentration of impurities was checked by ICP at Department of Chemistry, Faculty of Science, Masaryk University Brno, Czech Republic. Results of the analysis are listed in Table 1.

2.3. Corrosion experiments

Each sample ($2 \times 5 \times 7$ mm^3) of the investigated material was sealed into an ampoule made from the same material as the respective sample together with the mixture of solid batch of salts. The inner diameter of the ampoule was about 1.6 cm, the volume of the salt batch was about 18.4 cm^3. The ampoule was evacuated (residual pressure ~ 10 Pa) and then heated to 473 K/2 h for degassing. After this treatment, the ampoule was filled with Ar (pressure ~ 0.2–0.3 MPa, purity 4N8, concentration of residuals in vol.ppm: $O_2 \leq 3$, $H_2O \leq 5$, $N_2 \leq 10$) and tempered to the test temperature 953 K. Temperature of samples was registered with thermocouple Pt/Pt10Rh that was put in thermal contact from outside to the ampoule. After the salt mixture had melted (melting temperature $T_m = 925$ K), the sample was plunged into the bath with a manipulator and moved periodically up and down in the melt to simulate the flux of the coolant in the pipeline (quasi-dynamic regime of sample exposition). The mean velocity of the movement was 0.03 m s^{-1}. After the isothermal exposition (100, 300 and 1000 h), the samples were pulled up from the bath and cooled inside the ampoule to the room temperature.

2.4. SEM observations

The samples were pressed into Mounting Resin 4 (Diallyl green – Struers) and one of their front sides (2×5 mm^2) was ground and metallographically polished with diamond paste (last grain 3 μm). For the structure observation, the polished surface was etched in HCl (100) – H$_2$SO$_4$ (5) – CuSO$_4$ (20) at room temperature for 10 s; for X-ray microanalysis, the samples were not etched. For the SEM study, the surfaces were finally sputter coated by carbon to ensure the electric surface conductivity of the resin holder. The observations were done with SEM JEOL 6460 equipped with EDAX/WDAX analysers by OXFORD INSTRUMENTS.

2.5. XRD measurements

The phase composition of exposed surfaces of F was obtained by RTG diffraction method (XRD). The XRD profiles were obtained by X'Pert Pro MPD device (PANanalytical B.V., Almelo, the Netherlands) using Co Kα radiation and interpreted by the High-Score Plus software with commercial databases [28–30].
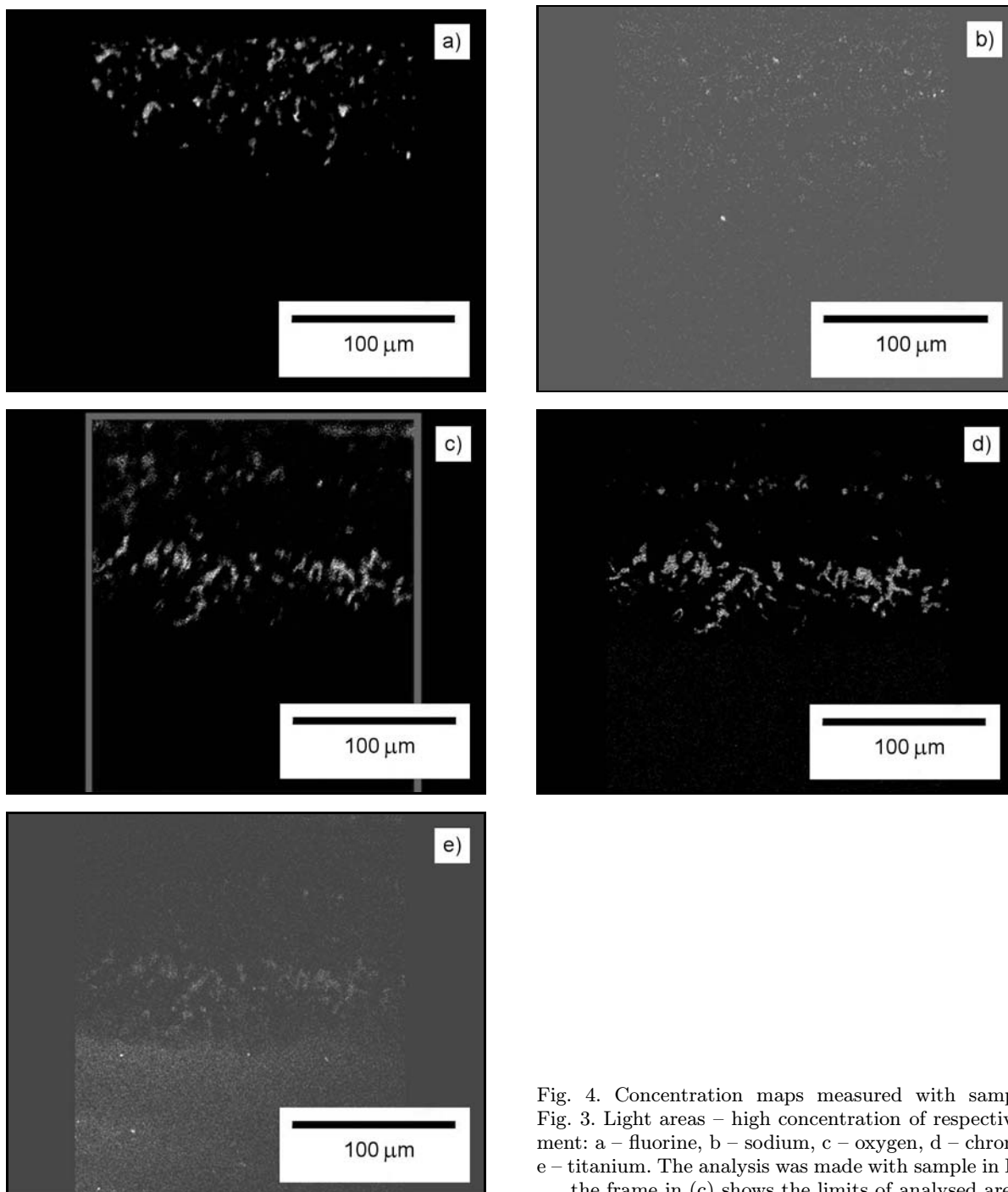
Fig. 4. Concentration maps measured with sample in Fig. 3. Light areas – high concentration of respective element: a – fluorine, b – sodium, c – oxygen, d – chromium, e – titanium. The analysis was made with sample in Fig. 3; the frame in (c) shows the limits of analysed area.

3. Results and discussion

3.1. Samples N

3.1.1. Structure

After the exposition of alloy N, corrosion damaged surface area of total thickness about 100–120 µm was observed – see Fig. 3. Total thickness of the area did not depend significantly on the duration of the corrosion test. Below the thin surface layer 1 (~ 5 µm)

that was almost without any pores, a porous layer was observed. Two types of pores were found: the larger ones forming a net of mutually connected pores (open porosity – areas 2, 3) close to the surface and smaller pores in greater depth (area 4).

3.1.2. 2D mapping of chemical composition

Results of mapping are illustrated in Fig. 4. It was found that the corrosion-damaged area (1–4 in Fig. 3) contains elements from the salt bath: besides fluorine
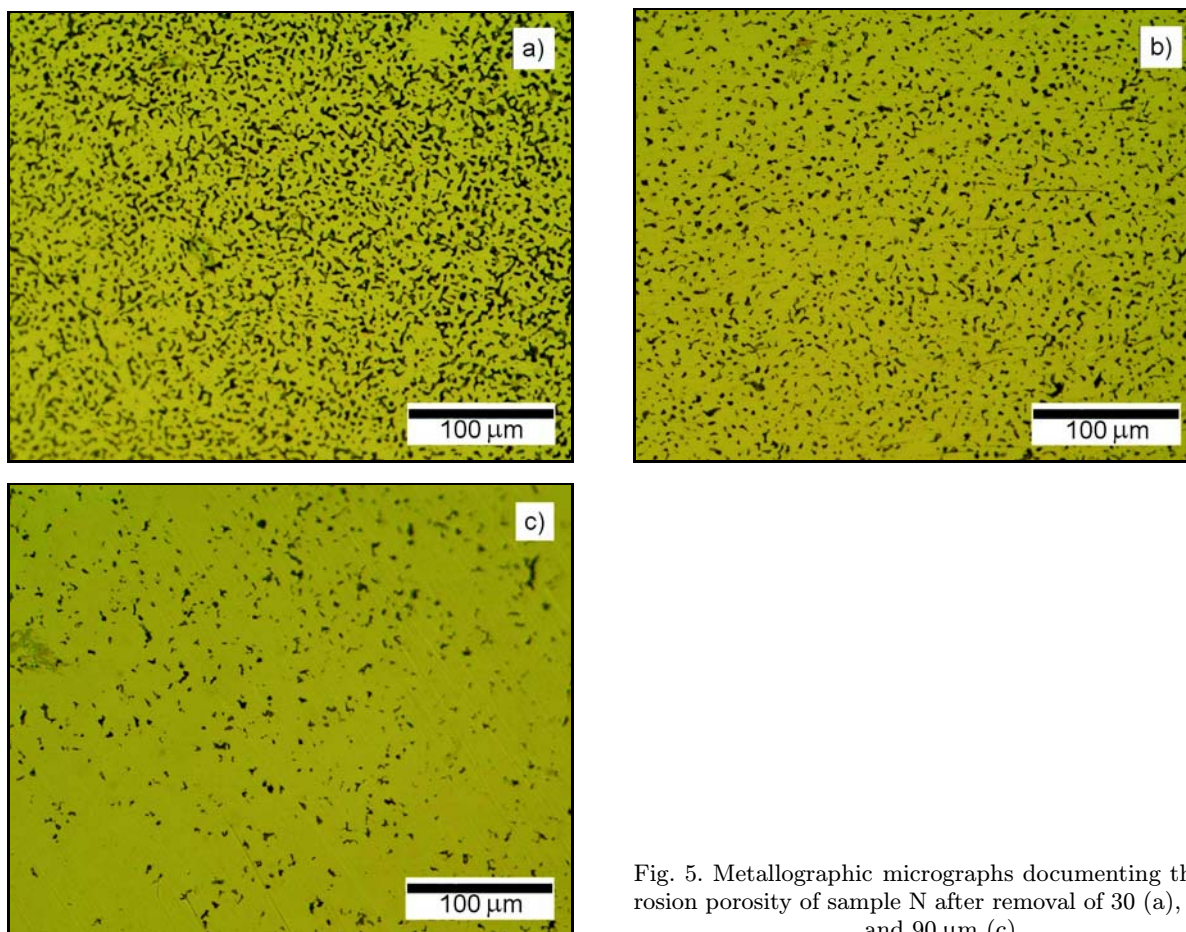
Fig. 5. Metallographic micrographs documenting the corrosion porosity of sample N after removal of 30 (a), 60 (b) and 90 µm (c).

(a) and sodium (b) also oxygen (c) were detected. The latter element is present in the salt bath as an impurity originating, most likely, from Ar used for the rinsing the ampoule before the corrosion experiment.

Large pores can be observed with dominant fluorine content in areas and traces of sodium inside (areas 2, 3 in Fig. 3, Fig. 4a,b), whereas in greater depth (area 4 in Fig. 3), narrow pores appeared with relative high content of Cr and Ti (Fig. 4d,e). A detailed analysis revealed that maximum in Ti and Cr concentration coincided with the deeper maximum of oxygen concentration. Moreover, the superposition of concentration maps for those elements supported the idea that Ti and Cr form oxide particles in the depth about 90–120 µm. The location of oxide particles coincides with smaller closed pores. The greater open pores contain a mixture of oxides of Cr (see the near-surface maximum in oxygen and Cr concentration) and fluorides. It was also found that the attacked surface layer was depleted on W and Mo.

Combined EDAX/WEDAX analysis led to a conclusion that the pores were nucleated preferentially in inter-dendrite matrix that was slightly depleted on W and enriched on Ti and Mo. Detrimental effect of Mo was reported also in [31], where the authors investigated the corrosion behaviour of Ni-based alloys in molten LiF + NaF salts and concluded that Mo tended to formation of precipitates and corrosion channels.

3.1.3. X-ray phase microanalysis

XRD study was done to estimate the *phase* composition of the attacked layer. The measurement of XRD profiles was carried out after the corrosion experiment (953 K/300 h) at the free surface and at three inner planes obtained by grinding-off the plan-parallel surface layers of total thickness 30, 60 and 90 µm (Fig. 5). Results are shown in Figs. 6, 7. It was found that there was considerable amount of LiF and NaF in great open pores. This conclusion was supported also by X-ray microanalysis and by mapping of chemical composition (see Fig. 4) that revealed very high concentration of fluorine in the pores. Intensity of peaks related to LiF and NaF decreased with increasing distance of the free surface that can be rationalized by decreasing porosity – see Fig. 5. As can be seen in Fig. 4, presence of chromium oxides was also detected, which was also supported by X-ray microanalysis (Fig. 7).

An attempt was done with the help of SW package [28–30] to identify not too expressive peaks that could not be assigned definitely to any phase. The results
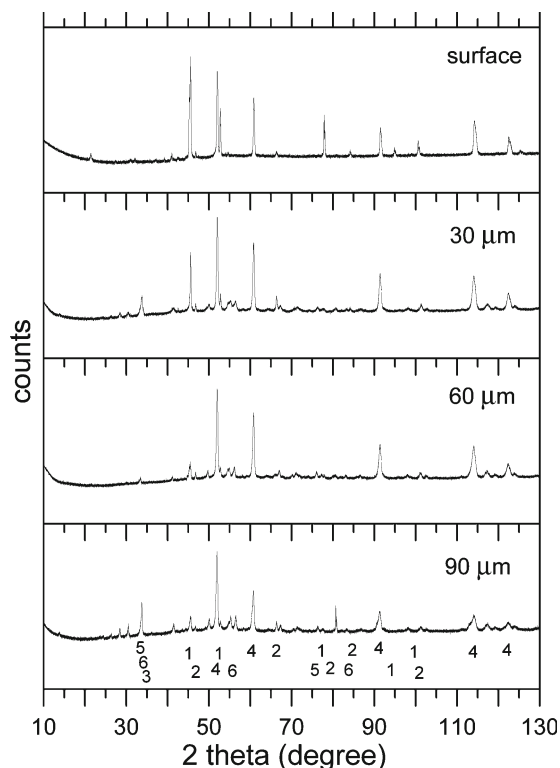
Fig. 6. XRD pattern of sample N taken at the surface and after the removal of 30, 60 and 90 μm. 1 – LiF, 2 – NaF, 3 – Na, 4 – Ni, 5 – CrO_2, 6 – Cr_3O_4.
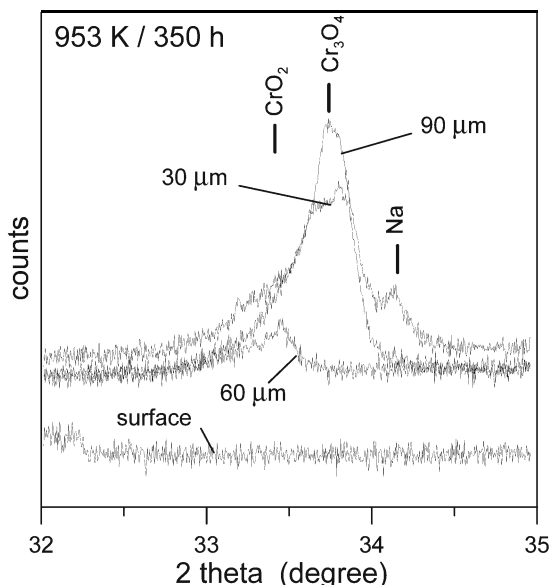

Fig 7. Detail of XRD pattern measured with the sample N before the grinding (surface) and after removal of 30, 60 and 90 μm.

led to a conclusion that in the large pores following fluorides might be present in a trace quantity: NiF_2, NiF_3, WF_6, Na_2NiF_6, $NaNiF_3$, $NaMoF_6$, and $NaWF_6$.

3.1.4. Corrosion mechanism of alloy N

It is known [32, 33] that LiF and NaF are very stable (Gibbs energies of formation are −29.9 and −30.8 kJ mol^{-1} of fluorides respectively at 1000 K). Therefore, they do not dissolve metallic components of attacked alloys too intensively. To start the corrosion process, some metallic elements have to be first oxidized to metallic fluorides M_mF_n according to schematic equation

$$m\,M + n\,A\,\mathrm{F} \longrightarrow M_m\mathrm{F}_n + n\,A, \qquad (3)$$

where M and A stand for metallic element and Li or Na, respectively. Metallic fluoride is then dissolved in coolant salt mixture LiF + NaF and may be carried away in the flowing bath. The Gibbs energy of formation of MoF_6, WF_6, NiF_2, CrF_2, and TiF_4 (–12.0, –13.6, –13.2, –18.0, and –20.4 kJ mol^{-1} of fluoride respectively at 1000 K [32]) is much greater than that for LiF and NaF (–29.9 and –30.8 kJ mol^{-1} of fluoride respectively at 1000 K [32, 33]).

Presence of oxygen may also lead to a formation of very stable oxides TiO_2, Cr_mO_n (–41.8 and about –30 respectively [34]).

Observed structure and chemical composition are illustrated in Fig. 4. It can be rationalized in terms of diffusion of elements into the alloy and as a result of parallel formation of metallic fluorides and oxides: The molecules LiF and NaF are dissociated in the melt [24–26] and fluorine, together with oxygen diffuse into the alloy. Diffusion of Na and probably also Li is – due to atomic size factor – much slower. When the concentration ratio of F and M (deeper than ca 5 μm – areas 2, 3 in Fig. 3) reaches the optimum value, M_mF_n is formed and subsequently dissolved in the mixture of LiF + NaF that penetrates into new-generated net of pores via cracks at the surface. In greater depths where the concentration of fluorine is low (area 4 and partly also area 3 in Fig. 3), the most stable oxides of Ti and Cr are formed preferentially.

3.2. Samples F

3.2.1. Structure

Micrographs of Ni-coated steel before the corrosion experiment are presented in Fig. 2. Needle-like Ni grains with longer axes perpendicular to the surface, well adhering to the steel substrate, were grown by Ni electrodeposition. During the corrosion experiments, the structure of both the Ni layer and the originally planar interface changed (Fig. 8): the Ni needle-like grains transformed to polygonized, equiaxed grains with the mean size of about 30 μm. Close to the original interface between the original Ni layer and the substrate (O.I.), the fine grained
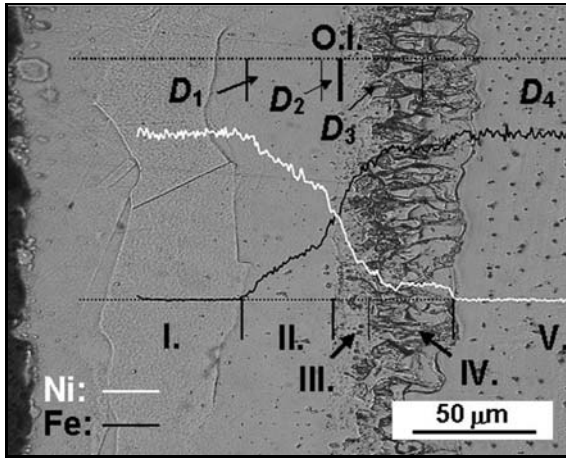
Fig. 8. Micrograph of sample F after corrosion test 953 K/1000 h. Left – Ni layer; right – steel substrate; left margin – free surface. I.–V.: metallographically distinguishable areas; D_1–D_4: diffusion coefficients describing the redistribution (see text); O.I.: original interface; superimposed lines: measured concentration of Ni and Fe.

Fig. 9. Concentration X_{Fe} and $(1 - X_{Ni})$ measured by SEM after corrosion tests of sample F.

interlayer (with thickness in tens of microns) appeared.

The mean grain size of the steel shows no significant changes during the corrosion exposition.

3.2.2. Diffusion across the O.I.

During the corrosion tests the samples behaved as a binary diffusion couple Ni-Fe since presence of C, Mn, Si in the steel did not affect the diffusion of Fe and Ni through the interface considerably.

Curves shown in Fig. 9 describe the redistribution of the both independently measured elements (i.e., $X = X_{Fe}$ and $X = 1 - X_{Ni}$; X – mole fractions) in dependence on distance x–ξ from the O.I. (ξ – co-ordinate of O.I.). It was found that the measured curves could be analysed into four distinct segments ascribed to metallographically well distinguishable areas (Fig. 8): Near-surface area I. with large polygonized approximately equiaxed Ni grains, area II. with γNi-Fe grains, with longer axes parallel with O.I., area III. with very fine γNi-Fe grains, area IV. with small columnar γNi-Fe grains oriented perpendicular to O.I. and area V. with ferritic steel.

The observed microstructure corresponds to segments found on measured redistribution curves: very slow diffusion in I. (concentration changes are below the detection limit), the first segment of the curves is in II., the second one is in area III. and reaches up to O.I., the third one starts at O.I. and reaches into IV. The last segment can be ascribed to diffusion in ferrite steel. Due to small grain size in areas III. and IV., the influence of grain boundary diffusion can be expected. Therefore, the break point between the third segment
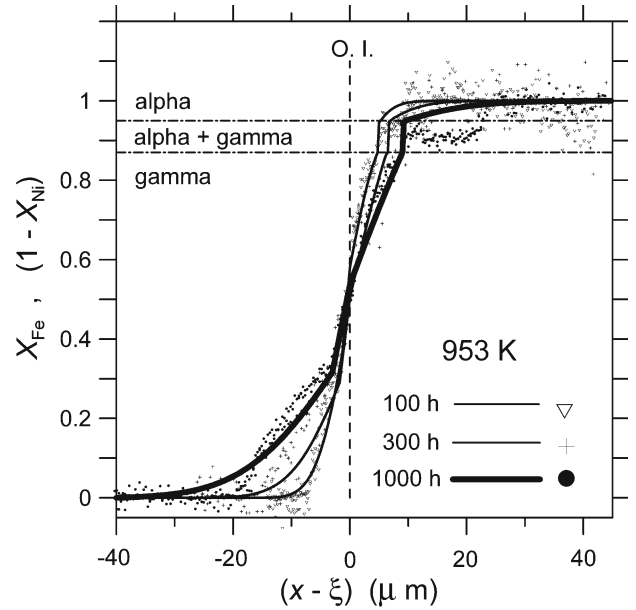
(significant contribution of grain boundary diffusion) and fourth one (volume diffusion in grains dominates) cannot be identified with any interface in the micrograph.

3.2.3. Diffusion model

Diffusion model was proposed for interpretation and/or prediction of chemical composition in the vicinity of the Ni protective surface layer in samples F. It comes

(i) from experimental fact that redistribution curves can be described by four chemical diffusion coefficients D_1–D_4 (Fig. 8),

(ii) from the thickness $\xi_{1/2}$, $\xi_{3/4}$ of areas dominated by D_2 and D_3, respectively (Fig. 8), measured independently and

(iii) from the existence of concentration discontinuity due to two-phase region $\alpha + \gamma$ [35–37].

Evolution of concentration X_{Fe}, $1 - X_{Ni}$ (X – mole fractions dependent on the distance from the O.I. and on time) was obtained numerically by finite difference method with time dependent position of interfaces described by parabolic law [38] and with condition of continuity of diffusion flux at all interfaces. At interfaces 1/2 and 2/3, continuity of X was kept, whereas at interface 3/4, values $(X_{Fe})_3 = [1 - (X_{Ni})_3] = 0.87$ and $(X_{Fe})_4 = [1 - (X_{Ni})_4] = 0.95$ [35] were fixed.

3.2.4. Results obtained using the model

The results of the *finite difference* simulation carried out using our own code are shown as full lines in Fig. 9. Optimal fit between the simulated solution
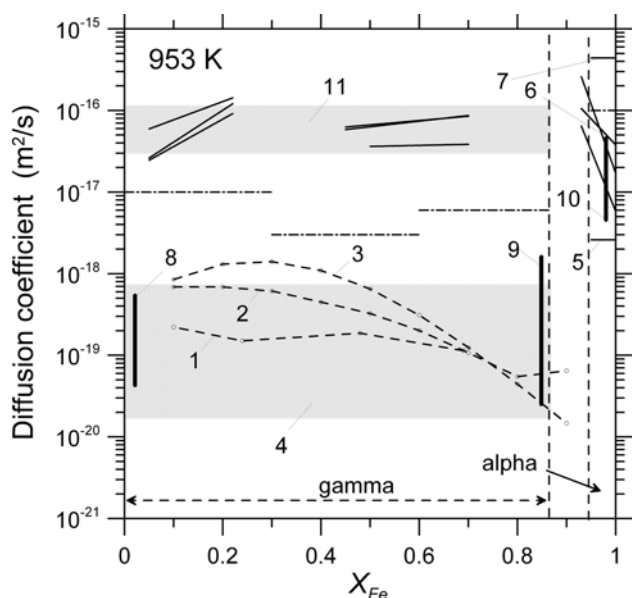
Fig. 10. Diffusion coefficients D_1–D_4 (dash-and-dot) obtained by optimisation of numerical model of mutual diffusion in sample F; concentration dependence of mutual diffusion coefficient obtained by Boltzmann-Matano analysis (full straight lines); mutual diffusion in γ-Fe-Ni: 1 – [42], 2 – [43], 3 – [44], in austenitic steels: 4 – [45–49], in α-Fe-Ni: 5 – [44], in ferritic steels: 6 – [50], 7 – [51], tracer diffusion in Ni: 8 – [52–54], in γ-Fe: [55], in α-Fe: [56–58]. 11 – effective diffusion coefficient in matrix with dislocations – see text.

and *all* measured data was achieved for values $\omega_{1/2}$ = $3 \times 10^{-9}\,\mathrm{m\,s^{-1}}$, $\omega_{3/4} = 1.5 \times 10^{-8}\,\mathrm{m\,s^{-1}}$, $D_1 = 1 \times 10^{-17}\,\mathrm{m^2\,s^{-1}}$, $D_2 = 3 \times 10^{-18}\,\mathrm{m^2\,s^{-1}}$, $D_3 = 5.6 \times 10^{-18}\,\mathrm{m^2\,s^{-1}}$ and $D_4 = 1 \times 10^{-16}\,\mathrm{m^2\,s^{-1}}$. It can be seen that the simulated profiles fit the data reasonably. The model offers a possibility to estimate concentration distribution of both Fe and Ni in the sample with reasonable accuracy.

However, it is also clear that the simulated profile does not describe properly the data in regions I., II. and IV. (cf. measured points with calculated lines in Fig. 9). It is caused, most likely, by the influence of short-circuit diffusion (dislocations in II. and grain boundaries in IV.).

Moreover, obtained values of D_1 through D_3 are much higher than literature data reported for similar measurements in Ni and in γNi-Fe. For comparison see Fig. 10, where present results are plotted together with literature data. On the other hand, present results obtained in ferrite agreed reasonably with scattered literature data on mutual and tracer diffusion in αNi-Fe and in αFe.

3.2.5. Boltzmann-Matano analysis
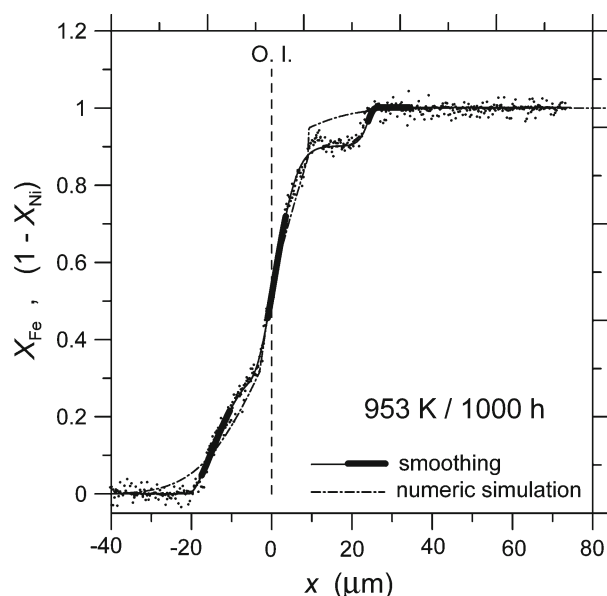
As mentioned above, numerical solution does

Fig. 11. One of redistribution curves measured after corrosion test 953 K/1000 h in sample F (points). Dash-and-dot line: numeric simulation; full line: smoothing with [40]. Bold segments were used for calculation of diffusion coefficients plotted in Fig. 10.

not account for influence of short-circuit paths. Therefore, the redistribution curves were evaluated also by Boltzmann-Matano analysis [39] that offers concentration-dependent chemical diffusion coefficient. The latter is inherently *effective*, which means that it accounts for contribution of high-diffusivity paths at given place x and in specific diffusion time t.

The fit quality is much better than in case of numerical simulation that did not account for the effect of short-circuit diffusion paths (Fig. 11). Diffusion coefficient $D(X_{\mathrm{Fe}})$ at co-ordinate x' with composition $X_{\mathrm{Fe}}(x')$ was obtained from the equation [38]

$$D(X_{\mathrm{Fe}}) = -\frac{1}{2\,t}\left[\frac{\partial x'}{\partial X_{\mathrm{Fe}}}\right]_{X_{\mathrm{Fe}}} \int_0^{X_{\mathrm{Fe}}} x'\,\mathrm{d}X_{\mathrm{Fe}}\,, \qquad (4)$$

where the derivative and the integral were evaluated numerically. Co-ordinate x' is related to Matano interface.

Similarly as values of D from numeric simulation, also values of $D(X_{\mathrm{Fe}})$ are much greater than literature data reported for diffusion measurements in Ni, γNi-Fe alloys and in austenitic steels – see Fig. 10.

To estimate the influence of diffusion along dislocations upon the values of D and $D(X_{\mathrm{Fe}})$ (it may be expected since the test temperature 953 K is below the $1/2$ of the melting temperature), one can use diffusion coefficients in dislocation core reported in [40], radius of dislocation core $a = 5$ Å [41] and typical dislocation
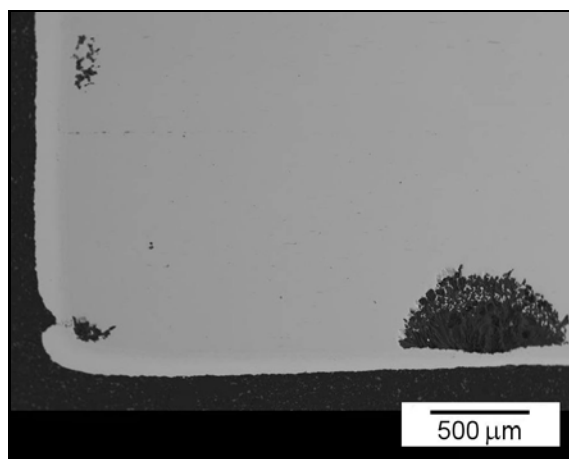
Fig. 12. Illustration of evolution of hemisphere-like corrosion damage in sample F.

density in Ni about $\rho = 10^{13}\,\mathrm{m}^{-2}$. Then effective diffusion coefficient from Hart's equation [41] can be estimated. It is obvious in Fig. 10 that estimated values (shaded area 11) overlap the present values of $D(X_{\mathrm{Fe}})$. The uncertainty of the effective diffusion coefficient is given before all by probable uncertainty in ρ.

Obtained values of $D(X_{\mathrm{Fe}})$ in α phase agree reasonably both with coefficient D obtained by numerical simulation and literature data. Relatively strong concentration dependence of $D(X_{\mathrm{Fe}})$ observed in the present work in α structure may explain considerable scatter of literature data.

3.2.6. Failure of protective effect of the Ni surface layer

It is illustrated in Fig. 8 that no damage of Ni layer is caused by the salt bath during the corrosion tests. Nevertheless, sporadic failures of catastrophic character were observed at places where the Ni layer was not perfect already before the corrosion test. It seems that these are the places where the layer is too thin or where it is cracked or perforated. Such a place serves as a starting point for progressive severe hemisphere-like failure, see Fig. 12. It was found that integrity of protecting Ni layer was frequently violated in the vicinity of edges, but it can be seen in Fig. 12 (right-hand-side of the micrograph) that the catastrophic failure can occur also at flat surface.

4. Summary

Corrosion behaviour of chosen materials for components used in molten salts technologies in the field of nuclear power generation was studied in the present

paper. Two types of samples were subjected to corrosion tests: Ni-based alloy (N) and Ni-covered steel CSN 411523 (F). The corrosion tests were done at temperature 953 K by dipping the samples into melted salt mixture LiF + NaF (60 : 40 mol.%). They were carried out in a quasidynamic regime simulating the flow of cooling media in the real pipeline system for three times: 100, 300 and 1000 h.

Corrosion damage of N was observed in a surface layer of thickness about 100–120 μm. If the bath contains oxygen as an impurity, closed pores are generated in the layer filled with chromium and titanium oxides. The major type of corrosion damage of N is, however, open porosity filled with melted salt mixture. Nucleation of the both types of pores occurs preferentially in inter-dendrite matrix that was originally slightly depleted on W and enriched on Ti and Mo. It seems likely that chromia-containing pores are formed as an initial stadium of corrosion damage followed – after the solution of chromia particles in the salt mixture – by the opening the pores and filling with the melt.

It was found that the Ni surface layer protected successfully the steel CSN 411523. Rapid attack of the steel was observed at those places only, where the Ni layer was cracked or too thin.

Coefficients of mutual diffusion between the steel and Ni layer was evaluated. It was found that the mutual diffusion in γ-Ni-Fe (i.e., in concentration range $X_{\mathrm{Fe}} = 0$–0.87) occurred much faster than it could be expected on the base of literature data known for diffusion in austenitic steels and for FCC Ni-Fe alloys. It was concluded that the most likely cause might be the short-cut diffusion along dislocations. Diffusion in the fine-grained layer close in the vicinity of I.O. is influenced by rapid diffusion along grain boundaries.

Obtained diffusion coefficients in α-Ni-Fe (i.e., in concentration range $X_{\mathrm{Fe}} = 0.95$–1) agree reasonably with literature data reported by other authors for α-Fe and for ferrite steels.

Simple model describing the diffusion of elements through the interface between the Ni layer and the steel was proposed. It was based on metallographic observation of the interface revealing four distinct layers that should be described by four diffusion coefficients. The model can be used for approximate calculation of chemical composition in surface layer of sample F.

References

[1] HOFFELNER, W.: Chimia, *59*, 2005, p. 977.

[2] KUNITOMI, K.—YAN, X.—NISHIHARA, T.—SAKABA, N.—MOURI, T.: Nucl. Eng. Technol., *39*, 2007, p. 9.

[3] FUKUDA, G. T.—PETERSON, P. F.—OLANDER, D. R.—PRAUSNITZ, J. M.: Fluid Phase Equilibria, *255*, 2007, p. 1.

[4] KUDRMAN, J.—ČMAKAL, J.—NEDBAL, I.—SIEGL, J.: Kovove Mater., *37*, 1999, p. 412.

[5] KUDRMAN, J.—ČMAKAL, J.—NEDBAL, I.—SIEGL, J.: Kovove Mater., *38*, 2000, p. 29.

[6] LAPIN, J.: Kovove Mater., *40*, 2002, p. 209.

[7] SCRIVANI, A.—RIZZI, G.—BARDI, U.: Kovove Mater., *43*, 2005, p. 382.

[8] CABET, C.—THIEBLEMONT, F.—GUERRE, C.: Materials and Corrosion – Werkstoffe und Korrosion, *59*, 2008, p. 591.

[9] BOČA, M.—CIBULKOVÁ, J.—KUBÍKOVÁ, B.—CHRENKOVÁ, A.—DANĚK, V.: J. Molecular Liquids, *116*, 2005, p. 29.

[10] HONG, S. G.—GREENSPAN, E.: Progress in Nuclear Energy, *47*, 2005, p. 239.

[11] ZHENG, C. L.—LI, J.—ZHOU, T.: Oxidation of Metals, *64*, 2005, p. 207.

[12] LI, M. H.—SUN, X. F.—HU, W. Y.—GUAN, H. R.—CHEN, S. G.: Oxidation of Metals, *65*, 2006, p. 137.

[13] FRANGINI, S.—LORETI, S.: Corrosion Science, *49*, 2007, p. 3969.

[14] GONZALEZ-RODRIGUEZ, J. G.—SALAZAR, M.—LUNA-RAMIREZ, A.—PORCAYO-CALDERON, J.—ROSAS, G.—VILLFANE, A. M.: High Temperature Materials and Processes, *23*, 2004, p. 177.

[15] MOHANTY, B. P.—SHORES, D. A.: Corrosion Science, *46*, 2004, p. 2993.

[16] SHORES, D. A.—MOHANTY, B. P.: Corrosion Science, *46*, 2004, p. 2909.

[17] ZHENG, C. L.—LI, J.—LIU, G. M.: High Temperature Materials and Processes, *26*, 2007, p. 167.

[18] TRISTANCHO, J.—VASQUEZ, C.—PENA, D.: DYNA-Colombia, *74*, 2007, p. 119.

[19] TZVETKOFF, T.—GIRGINOV, A.: J. Mater. Sci., *30*, 1995, p. 5561.

[20] SEQUEIRA, C. A. C.: Molten Salt Forum, *7*, 2003, p. 3.

[21] IGNATEV, V. V.—SURENKOV, A. I.—GNIDOI, I. P.—FEDULOV, V. I.—UGLOV, V. S.—PANOV, A. V.—SAGARADZE, V. V.—SUBBOTIN, V. G.—TOROPOV, A. D.—AFONICHKIN, V. K.—BOVE, A. L.: Atomic Energy, *101*, 2006, p. 730.

[22] WILLIAMS, D. F.: Assessment of Candidate Molten Salt Coolants for the NGNP/NHI Heat Transfer Loops. ORNL/TM-2006/69. Oak Ridge, TN, Oak Ridge National Laboratory 2006.

[23] WILLIAMS, D. F.—TOTH, L. M.—CLARNO, K. T.: Assessment of Candidate Molten Salt Coolants for the Advanced High-Temperature Reactor (AHTR). ORNL/TM-2006/12. Oak Ridge, TN, Oak Ridge National Laboratory 2006.

[24] BARTONÍČEK, R. et al.: Koroze a protikorozní ochrana kovů (Corrosion and Anticorrosion Treatment of Metals). Praha, Academia 1966 (in Czech).

[25] NIANUI, C.—HUA, X.—JUN, S.: ACTA Physico-Chimica Sinica, *4*, 1988, p. 451 (English version).

[26] KOURA, T.—MATSUURA, H.—OKADA, I.: J. Molecular Liquids, *73–74*, 1997, p. 195.

[27] MATAL, O.—ŠIMO, T.—NESVADBA, L.—DVOŘÁK, V.—KANICKÝ, V.—SULOVSKÝ, P.—MACHÁT, J.: Zeitschrift für Naturforschung Section A – J. Phys. Sci., *62*, 2007, p. 769.

[28] ICSD Database release 2007/1, FIZ Karlsruhe, Germany.

[29] JCPDS PDF-4 Full File 2004 Database, ICDD, Newton Square, Pennsylvania, U.S.A.

[30] X'Pert HighScore Plus 2.0a, PANanalytical B.V., Almelo, the Netherlands.

[31] BRENNER, O.—CIZNER, J.—KASL, J.—JANDOVÁ, D.: In: Proc. 17th International Metallurgical & Material Conference METAL 2008. Ostrava, Tanger 2008, No. 221 (on CD-rom). ISBN 978-80-254-1987-8.

[32] CHENG, E. T.—MERRILL, B. J.—SZE, D. K.: Fusion Engineering and Design, *69*, 2003, p. 205.

[33] FORSBERG, C. V.—PETERSON, P. F.—ZHAO, H.: J. Solar Energy Engineering, *129*, 2007, p. 141.

[34] RICHARDSON, F. D.—JEFFES, J. H. E.: J. Iron Steel Inst., *160*, 1948, p. 261.

[35] MASSALSKI, T. B. (Ed.): Binary Alloy Phase Diagrams. ASM Internat., Metals Park, Ohio 44073 1996 (CD).

[36] CAHN, R. W.—HAASEN, P.: Physical Metallurgy. Amsterdam, Oxford, New York, Tokyo, North-Holland Physics Publ. 1983.

[37] ADDA, Y.—PHILIBERT, J.: La Diffusion dans les Solides. Saclay, Inst. National des Sciences et Techniques Nucleaires 1966.

[38] KIRKALDY, J. S.—YOUNG, D. J.: Diffusion in the Condensed State. London, The Institute of Metals 1987.

[39] WUTTIG, M.—BIRNBAU, H. K.: Phys. Rev., *147*, 1966, p. 495.

[40] TableCurve AISN Software, SPSS Inc. 1996.

[41] KAUR, I.—MISHIN, Y.—GUST, W.: Fundamentals of Grain and Interphase Boundary Diffusion. Chichester, New York, Brisbane, Toronto, Singapore, John Wiley & Sons 1995.

[42] FRADEN, F.: B. S. Thesis, M. I. T. (1963) – quoted from [34].

[43] USTAD, T.—SORUM, H.: Phys. Status Solidi (a), *20*, 1973, p. 285.

[44] YANG, J.—GOLDSTEIN, J. I.: Metall. Mater. Trans., *35A*, 2004, p. 1681.

[45] MILLION, B.—CÍHA, K.—STRÁNSKÝ, K.: Kovove Mater., *13*, 1975, p. 3 (in Czech).

[46] MILLION, B.—CÍHA, K.—STRÁNSKÝ, K.: Kovove Mater., *13*, 1975, p. 545 (in Czech).

[47] MILLION, B.: Kovove Mater., *14*, 1976, 490 (in Czech).

[48] MILLION, B.—CÍHA, K.—KRUMPOS, J.—STRÁNSKÝ, K.: Kovove Mater., *14*, 1976, p. 636 (in Czech).

[49] MILLION, B.: Kovove Mater., *18*, 1980, p. 154 (in Czech).

[50] CÍHA, K.—FOLDYNA, V.—KRUMPOS, J.—MILLION, B.—STRÁNSKÝ, K.: Kovove Mater., *19*, 1981, p. 517 (in Czech).

[51] KUČERA, J.—CÍHA, K.—MILLION, B.—STRÁN-SKÝ, K.: Kovove Mater., *25*, 1987, p. 671.

[52] MAYER, K.—MEHRER, H.—LESSMANN, E.—SCHUELE, W.: Phys. Status Solidi (b), *78*, 1979, p. 689.

[53] WAZZAN, A. R.: J. Appl. Phys., *36*, 1965, p. 3596.

[54] MONMA, K.—SUTO, H.—OIKAWA, H.: J. Japan Inst. Metals, Tohoku Univ., *28*, 1964, p. 188.

[55] Materials Database of Japan National Institute for Materials Science (NIMS); http://www.nims.go.jp

[56] KUČERA, J.—MILLION, B.—RUŽIČKOVÁ, J.: Phys. Status Solidi (a), *96*, 1986, p. 177.

[57] CHONGMO, L.—HILLERT, M.: Acta Metall., *29*, 1981, p. 1949.

[58] HIRANO, K.—COHEN, M.—AVERBACH, B. L.: Acta Metall., *9*, 1961, p. 440.